Crystal Structures of the S_{MK} box (SAM-III) Riboswitch Reveal the SAM-dependent Translation Inhibition Mechanism

Supplementary Information

Changrui Lu[*], Angela M. Smith[†], Ryan T. Fuchs[†], Fang Ding[*], Kanagalaghatta Rajashankar[‡], Tina M. Henkin[†], Ailong Ke[*§]

[*]Department of Molecular Biology and Genetics, Cornell University, Ithaca, NY 14853
[†]Department of Microbiology and Center for RNA Biology, Ohio State University, Columbus, OH 43210
[‡] NE-CAT, Advanced Photon Source, Argonne, IL 60439

[§]**To whom correspondence may be addressed:**
Ailong Ke: Department of Molecular Biology and Genetics, 251 Biotechnology Building, Cornell University, Ithaca, NY 14853, USA; Phone: (607) 255-3945; FAX: (607) 255-6249; e-mail: ailong.ke@cornell.edu

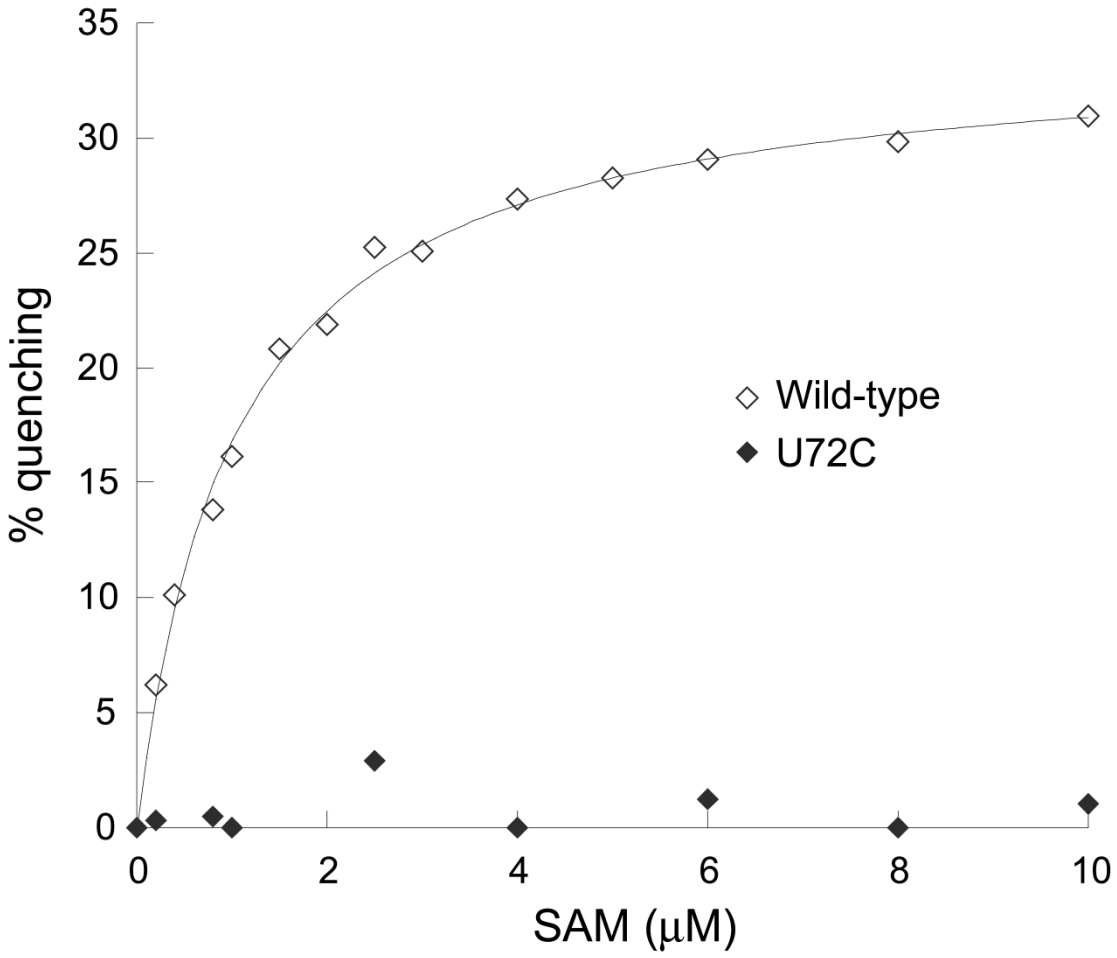

Supplemental Figure 1. 2-AP fluorescence quenching in response to SAM. Increasing concentrations of SAM were added to bipartite *metK* leader RNA containing an internal 2-AP modification at residue A29. 2-AP fluorescence at steady-state was measured at 375 nm with an excitation wavelength of 310 nm. Increasing SAM resulted in quenching of 2-AP fluorescence for the wild-type RNA (open diamonds), but no substantial change in fluorescence was observed with a U72C mutant RNA (closed diamonds) that is predicted to bind SAM very poorly. Percent quenching ($\Delta F/F_0$ x 100) represents the change in fluorescence normalized to the initial fluorescence observed in the absence of SAM. Data were analyzed by nonlinear regression analysis to determine an apparent K_d of 1.0 μM for the wild-type RNA.

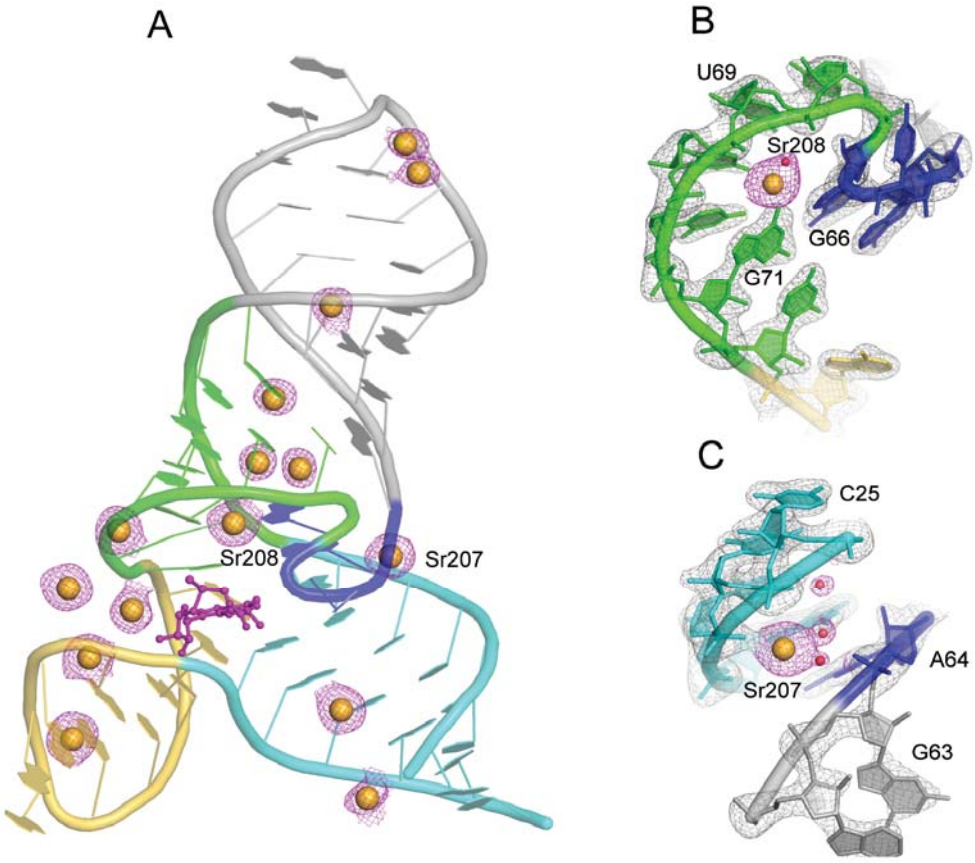

Supplemental Figure 2. Metal binding sites in the S_{MK} box RNA. (A). Overall view of the fifteen strontium binding sites on the S_{MK} box RNA. (B, C). Electron density map (grey mesh) showing two strontium ions (Sr208 and Sr207) bound to their respective sites on the S_{MK} box RNA. The magenta mesh shows the simulated composite omit electron density map of strontium contoured at 1 σ. Yellow ball, strontium ion; red ball, water. The coloring scheme for the RNA is consistent with that in Figure 1.

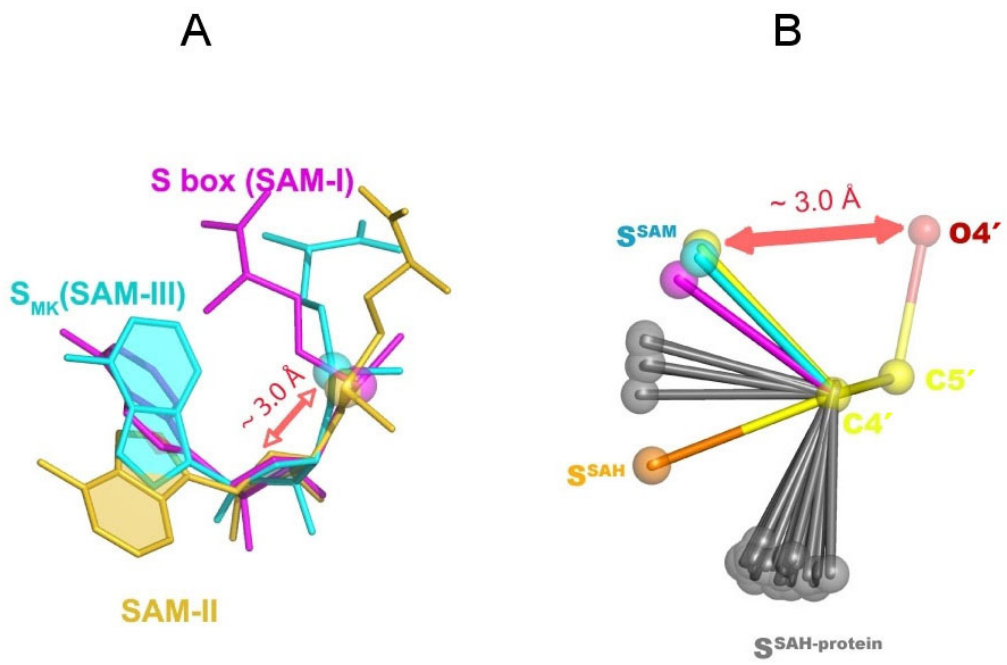

Supplemental Figure 3. Conformational comparison between SAM and SAH molecules in various riboswitch and protein structures. (A). SAM conformation from all three classes of SAM riboswitches, aligned along the ribose portion. Despite conformational differences in the adenosine base and the methionine tail, the sulfur atom makes a constant 3.0 Å polar interaction with the O4′ of the ribose. (B). Comparison of the O4′-C4′-C5′-S dihedral angle within the SAM and SAH molecules. Molecules are aligned along the O4′-C4′-C5′ linkage. *Gauche* conformation about the C4′-C5′ bonds (labeled S^{SAM}) is the predominant conformation of SAM in the riboswitch complexes (the C5′-S bond is colored in yellow, cyan, and magenta for the S box (SAM-I), SAM-II and S_{MK} box [SAM-III] respectively). By contrast, a survey of 30 randomly chosen SAH-bound protein structures revealed that in 87% of the structures, the sulfur ($S^{SAH\text{-}protein}$) adopts the *anti* conformation (pointing towards the 6 o′clock position). SAH in our S_{MK} box structure adopts a near *anti* conformation (the sulfur atom is labeled S^{SAH} and colored in orange).

Supplementary Table 1. Analysis of Sr^{2+}-RNA interactions in the S_{MK} box riboswitch.

Divalent cation ID	Interacting base number	RNA ligand*	Metal-ligand Distance (Å)
Sr201	A27	O1P	4.7
Sr202	G91	O6	4.5
	G92	O6	4.3
Sr203	G30	O6	4.6
	G31	O6	4.3
Sr204	G88	O6	2.9
		N7	2.9
Sr205	A86	O1P	4.5
	G76	N7	4.4
Sr206	G47	O1P	3.5
	U45	O6	2.8
Sr207	C25	O1P	2.6
	A64	O2P	4.4
Sr208	G71	O6	2.8
	G66	O2P	4.4
	U69	O2P	3.0
	C68	O2P	4.6
Sr209	A73	O1P	2.8
	A27	N3	4.6
		O2'	4.4
Sr210	G71	O1P	4.7
	G88	O2P	4.7
	U72	O1P	4.8
Sr211	G47	O2P	4.7
	U45	N7	2.9
	A44	N7	4.4
Sr212	U69	O2'	3.7
	U70	O4'	4.0
Sr213	U33	O4	2.5
	U34	N6	3.0
	A61	N4	4.2
	U35	O6	4.2
	A60	N4	4.3

Sr214	G66	O6	4.4
	A27	O2P	4.4
	A28	N7	4.0
		O1P	4.5
Sr215	A73	O2P	2.4
	A74	O2P	3.3
		N7	4.6

* Inner-sphere Sr^{2+}-RNA interactions should be around 2.5 Å. In most of identified Sr^{2+} ions, the hydration shell is not resolved in the 2.2 Å electron density map. Thus, we list all RNA functional groups within 4.8 Å of Sr^{2+} ions as potential outer-sphere ligands.

SUPPLEMENTAL METHODS

RNA preparation and crystallization

We inserted the *E. faecalis* S_{MK} box riboswitch sequence into a pUC19 plasmid under the control of a T7 RNA polymerase (RNAP) promoter, with the hepatitis delta virus ribozyme placed at the 3′ end of the S_{MK} box sequence to ensure a homogeneous 3′-end. The crystallization construct initiates 1 nt upstream of the ASD sequence and ends 3 nucleotides (nt) downstream of the SD sequence. In the process of searching for better diffracting RNA crystals, the hypervariable P3 stem was replaced with a five bp GC-rich stem capped with a GAAA tetraloop, and the hypervariable linker connecting the SD sequence to the upstream helical domain was systematically shortened. Nine different constructs were generated by combining variations at two hypervariable regions (P3 and P4) [1].

Data collection and structure refinement

A microcrystallography setup was required to obtain high-resolution data sets from the S_{MK}6 needle crystals. Diffraction data were collected at beamlines APS 24-ID-E and MACCHESS F1. Due to very fast radiation decay, the needle crystals were aligned and transferred parallel to the oscillation axis to allow collection of complete data sets with satisfactory redundancy. Data were processed using HKL2000 [2].

While most S_{MK} crystals belong to the $I4_122$ space group [one molecule per asymmetric unit (ASU)], a few fall into the $P4_12_12$ space group with similar unit cell dimensions (two molecules per ASU). A 3.8 Å single wavelength anomalous diffraction data set was collected from a $P4_12_12$ crystal soaked in 80 mM iridium hexaammine. The initial phase calculated using program SHELXD [3] from eight iridium hexaammine sites was improved by applying a 2-fold noncrystallographic symmetry (NCS) to average the two molecules in ASU. Figure of Merit is 0.70, and R_{cullis} is

0.57(0.68 for the outer shell). After solvent-flattening and phase extension to a 2.6 Å native data set, the experimental density map allowed unambiguous model building of 23 nucleotides using program COOT [4]. 20 nucleotides were missing in the initial model, including the entire P3, J3/2, and part of P2. To locate the P3 helix, an ideal RNA model containing a 5-base pair A-form duplex capped by a GAAA tetraloop was included in the molecular replacement search using program PHASER [5]. The correct solution was identified from the top rotation and translation solutions after manual examination of the crystal packing environment. The rest of the missing nucleotides were added one or two bases at a time followed by restrained positional refinement using Refmac5 [6]. The SAM molecule was then real-space fitted into the difference map using COOT [4]. The completed structural model was refined against a 2.2 Å $I4_122$ native data set in iterative cycles of torsion-angle simulated annealing, group/individual B-factor refinement, and Powell energy minimization in CNS [7,8]. A final round of TLS refinement in Refmac5 was carried out to model domain movements within the RNA [6]. The same set of excluded reflections was used in free R factor calculation between refinement programs.

Determination of Se-SAM and SAH bound S_{MK} structures

A Se-SAM soaking experiment was used to confirm the sulfonium position in the S_{MK} box riboswitch. To introduce Se-SAM and titrate away bound SAM, S_{MK} crystals were exposed to Se-SAM (10 mM final concentration, freshly prepared and confirmed by mass spectrometry to be intact) during the entire cryoprotection procedure over the course of 2 hr. The crystals were first incubated and then sequentially transferred into three fresh Se-SAM solutions with increasing cryoprotectant concentration and incubated for at least 20 min between each transfer before snap-freezing in liquid nitrogen. 2.7 Å diffraction data sets were collected on the APS ID-24E microdiffraction beamline at the K absorption edge of Se. The native $S_{MK}6$ structure (excluding SAM, metal ions, and water coordinates) was used as the starting model for rigid body and

B-factor refinement in Refmac5 [6], followed by simulated annealing refinement in CNS [8] to remove model bias. The structural model was further refined in CNS [8] as described for the SAM-bound structure, and the Se-SAM model was introduced at the later stage of the refinement. The selenium atom in Se-SAM was located in the sigmaA-weighted anomalous difference Fourier map, where the only substantial peak overlaps with the selenium/sulfur position in the structure model. The final Se-SAM-bound $S_{MK}6$ structure contains fifteen strontium ions and eleven waters with R_{work}/R_{free} of 22.7%/25.5%.

To examine the binding of SAH, the $S_{MK}6$ crystal was repeatedly transferred into solutions containing a saturating amount of SAH (~2 mM) over the course of three days. The structure was solved using a molecular replacement method from a 2.9 Å data set collected at the microdiffraction beamline 24ID-E at APS. The refinement procedure was essentially the same as described for the Se-SAM structure. Final R_{work}/R_{free} is 22.2%/25.9%. We verified both structures using simulated annealing omit maps by excluding five bases in each calculation.

SUPPLEMENTAL RESULTS

K_d measurement by 2-AP fluorescence

To verify the apparent K_d value observed in the size-exclusion filtration experiment, a second assay was developed to test the binding affinity of SAM to the wild-type 15-118 *metK* leader RNA. For this we used a bipartite RNA comprised of two half RNAs, corresponding to positions 15-46 and 47-118. The two RNA halves are predicted to anneal through extensive base pairing in the P1-P3 helices to form the full-length *metK* leader RNA corresponding to positions 15-118, with a nick immediately upstream of residue G47 at the top of the P3 stem loop. A 2-aminopurine (2-AP) modification was incorporated into the upstream RNA at residue A29 to monitor local conformational changes occurring at this position in response to SAM binding using florescence spectroscopy. In the absence of SAM, sample excitation at 310 nm yielded a fluorescence emission peak at 375 nm. Addition of SAM resulted in a concentration-dependent quenching of 2-AP fluorescence that was not observed with addition of SAH (data not shown). SAM titrations were used to determine an apparent K_d value of 1.03 μM for the wild-type *metK* RNA (Figure 2C), which is in close agreement to the value obtained using the size-exclusion filtration assay. No quenching of 2-AP fluorescence was observed with an RNA construct containing a U72C substitution with SAM concentrations up to 100 μM (Figure 2C and data not shown), consistent with the loss of SAM binding to the U72C RNA in the filtration assay (Supplementary Fig. 1).

REFERENCES

1. Fuchs, R.T., Grundy, F.J. & Henkin, T.M. The S_{MK} box is a new SAM-binding RNA for translational regulation of SAM synthetase. *Nat. Struct. Mol. Biol.* **13**, 226-233 (2006).
2. Otwinowski, Z. & Minor, W. Processing of X-ray diffraction data collected in oscillation mode. *Methods Enzymol.* **276**, 307-326 (1997).
3. Sheldrick, G.M. A short history of SHELX. *Acta Crystallogr A* **64**, 112-22 (2008).
4. Emsley, P. & Cowtan, K. Coot: Model-building tools for molecular graphics. *Acta Crystallogr. D* **60**, 2126-2132 (2004).
5. Storoni, L.C., McCoy, A.J. & Read, R.J. Likelihood-enhanced fast rotation functions. *Acta Crystallogr. D* **60**, 432-438 (2004).
6. Collaborative Computational Project, N. The CCP4 suite: programs for protein crystallography. *Acta Crystallogr. D* **50**, 760-763 (1994).
7. Brunger, A.T. et al. Crystallography & NMR system: A new software suite for macromolecular structure determination. *Acta Crystallogr. D* **54**, 905-921 (1998).
8. Brunger, A.T. Version 1.2 of the Crystallography and NMR system. *Nature Protocols* **2**, 2728-2733 (2007).